Methacrylated silk fibroin hydrogels

Barroso, Inês A.; Man, Kenny; Villapun, Victor M.; Cox, Sophie C.; Ghag, Anita K.

DOI:
10.1021/acsbiomaterials.1c00791

Document Version
Peer reviewed version

Citation for published version (Harvard):
Barroso, IA, Man, K, Villapun, VM, Cox, SC & Ghag, AK 2021, 'Methacrylated silk fibroin hydrogels: pH as a tool to control functionality', *ACS Biomaterial Science and Engineering*, vol. 7, no. 10, pp. 4779-4791. https://doi.org/10.1021/acsbiomaterials.1c00791

Methacrylated Silk Fibroin hydrogels: pH as a tool to control functionality

Inês A. Barroso [1], Kenny Man [1], Victor M. Villapun [1], Sophie C. Cox [1], Anita K. Ghag [1*]

[1] School of Chemical Engineering, University of Birmingham, Edgbaston B15 2TT, Birmingham, United Kingdom

*Corresponding author: A.K.Ghag@bham.ac.uk

Ms Inês A. Barroso (IXP799@student.bham.ac.uk)
Dr Kenny Man (K.L.Man@bham.ac.uk)
Dr Victor M. Villapun (V.M.Villapun@bham.ac.uk)
Dr Sophie C. Cox (S.C.Cox@bham.ac.uk)
Dr Anita K. Ghag (A.K.Ghag@bham.ac.uk)

Abstract

The last decade has witnessed significant progress in the development of photosensitive polymers for *in situ* polymerisation and 3D printing applications. Light-mediated sol-gel transitions have immense potential for tissue engineering applications as cell-laden materials can be crosslinked within minutes in mild environmental conditions. Silk fibroin (SF) is extensively explored in regenerative medicine applications due to its ease of modification and exceptional mechanical properties along with cytocompatibility. To efficiently design SF materials, the *in vivo* assembly of SF proteins must be considered. During SF biosynthesis, changes in pH, water content and metal ion concentrations throughout the silkworm gland divisions drive the transition from liquid silk to its fibre form. Herein, we study the effect of glycidyl-methacrylate-modified SF (SilkMA) solution pH on the properties and secondary structure of SilkMA hydrogels by testing formulations prepared at pH 5, 7 and 8. Our results demonstrate an influence of the prepolymer solution pH on the hydrogel rheological properties, compressive modulus, optical transmittance and network swellability. The hydrogel pH did not affect the *in vitro* viability and morphology of human dermal fibroblasts. This work demonstrates the utility of the solution pH to tailor SilkMA conformational structure development towards utility and function and shows the need to strictly control pH to reduce batch-to-batch variability and ensure reproducibility.

Keywords: Silk, methacrylated silk, pH, hydrogel, β-sheet, regenerative medicine.

1. Introduction

Hydrogels have been extensively studied in the tissue engineering field due to their three-dimensional hydrophilic networks, biodegradability and elasticity [1],[2]. In particular, polypeptides (e.g. collagen, gelatin, silk) are particularly attractive due to their resemblance with the native extracellular matrix environment [3]. Recently, there is increasing interest in the development of photosensitive hydrogels for 3D printing and *in situ* polymerisation applications. These materials can be combined with cells, growth factors and bioactive factors and crosslinked within seconds using light. Despite these advantages, limited reproducibility and batch-to-batch variability remain the main preventive factors to the wide application of natural polymers in tissue engineering.

In the last decade, silk-fibroin (SF) has proved itself one of the most versatile materials available for regenerative medicine applications. Its water-based processing and ease of

modification along with exceptional mechanical properties, biocompatibility and slow *in vivo* degradation, makes it an attractive material for regenerative medicine [4][5]. Silks are naturally-derived fibrous proteins produced by spiders, silkworms, bees, moths and scorpions [6], [7]. The composition, structure and properties of silk extracted from different species are variable. Silk obtained from the *Bombyx mori* (domesticated silkworm) have been most extensively studied and used in textile production for more than 4000 years [8]. *Bombyx mor*i silk is composed of two main proteins: sericin (20-30%) and SF (70-80%) with trace amounts of carbohydrates and waxes [9]. Since sericin generally yields an inflammatory response, this protein is typically removed through a process called degumming [10].

To efficiently optimise SF materials and design synthetic polymers that mimic natural silk, the *in vivo* assembly of silk proteins must be understood [11]. *In vivo*, silk exhibits a water-soluble structure composed of random coil, α-helix, and hydrated β-strands. However, after spinning, SF assumes a remarkably stable and insoluble β-sheet crystalline structure stabilised by hydrogen bonds [11]. In the mulberry silkworm, *Bombyx mori*, the silk glands consist of a posterior, middle and anterior division followed by the spinning duct [11]. As liquid SF flows through the secretory pathway, changes in pH, water content and metal ion concentrations are thought to drive the transition from noncrystalline liquid silk to its fibre structure [11]. Foo et al. studied how variations in pH and salt concentrations throughout the silk glands affect the assembly of silk proteins during natural processing [11]. From the posterior to the anterior part of the secretory pathway, the pH decreases from 6.9 to 4.8. At near neutral pH, strong repulsive forces prevent protein-protein interactions due to the prevalence of negative charges [12]. As the acidity increases the hydrophilic spacers (pI = 4.03), L-chain (pI = 5.06) and the N-termini (pI = 4.59) and C-termini (pI = 10.53) of the H-chain become less negatively charged. The charge suppression by acidification allows hydrophobic and hydrophilic interactions to occur and initiates changes in the protein secondary structure [12][11]. Simultaneously, the water content falls from 88% to 70% and the cation concentration increases to neutralize the repulsion forces between the chains. This close packing is fundamental for proper folding and formation of micellar structures, which will then aggregate and form globular structures before being converted into fibres due to strain-induced β-sheet formation in the spinneret [11].

The majority of studies published to date concerning the development of SF materials are based on protein self-assembly into β-sheet-rich networks, referred to as physical crosslinking. Many

processes have been identified to induce β-sheet transition; decreased pH [7], [13], [14], high temperatures [15], [16], addition of Ca^{2+} ions [7], methanol/ethanol treatments [17]–[21] and direct electric currents [4], [22], [23]. Strong shear forces mimicking the natural silkworm spinning process also induce gelation (e.g. sonication [24], vortexing [25]). However, despite providing strength to the hydrogels through physical cross-linking, these β-sheet structures also result in brittle behaviour as the crystals block long-range molecular displacements [26]. Therefore, despite their high stiffness, these hydrogels lack the adequate elastic properties needed for the repair of many tissues (e.g. skin and cartilage) [3]. Furthermore, the protocols used to prepare physically crosslinked SF materials are incompatible with cell encapsulation due to long gelation times (from 30 minutes to several hours) and unsuitable environmental conditions, limiting the clinical application of these materials [3].

Over the last decade, efforts to develop chemically crosslinked SF hydrogels have been made [3], [26]. These materials have completely distinct properties when compared with the physically crosslinked hydrogels previously mentioned. Partlow et al. developed a highly elastic SF hydrogel using horseradish peroxidase (HRP) mediated crosslinking approach [26]. The gelation kinetics of these enzymatically crosslinked hydrogels can be tailored by changing the HRP and oxygen peroxidase (H_2O_2) content. Yan et al., prepared 16 wt% SF hydrogels with storage modulus between several hundred Pa to 5 kPa within 5 to 21 minutes, by changing the H_2O_2 concentration between 0.8 to 1.45‰ [3].

Recently, due to the increasing interest in 3D printing technologies, several polymers have been successfully chemically modified to allow photocrosslinking, such as collagen [27], gelatin [28]–[30], hyaluronan [31], [32], silk fibroin [33], alginate [31], dextran [34], PVA [28] or PEG [35]. Herein, we developed glycidyl-methacrylate-modified SF (SilkMA) hydrogels that can be prepared within minutes via free radical polymerisation (chemical crosslinking). Notably, cells can be encapsulated within the hydrogels and the physical properties of the hydrogels can be easily tailored by changing the degree of methacrylation (DM%), polymer concentration and the photoinitiator system [33].

Due to the novelty of SilkMA hydrogels, little is known about the role of the prepolymer solution pH in the initial and long-term properties of the gels. Given the importance of pH changes during *in viv*o processing, we hypothesise that it will influence the overall properties

of SilkMA gels and could be used to control the secondary structure towards functionality. The pH influence on the initial properties of SilkMA gels was studied in terms of physicochemical properties and cell behaviour. Finally, the spontaneous conformation transitions at physiological conditions and the mechanically toughening impact of β-sheet crystallinity were also addressed. This work highlights the need to rigorously control the pH of silk prepolymer solutions to enhance the reproducible manufacturing process, thereby increasing the potential clinical adoption of silk-based materials for numerous therapeutic applications.

2. Methods

2.1 Preparation of Methacrylated Silk Fibroin (SilkMA)

2.1.1 Silk Fibroin Extraction

Bombyx Mori cocoons were supplied by The Yarn Tree (Roanoke, USA). Each cocoon was sliced into four pieces and the silkworms were discarded. To remove the sericin, 10 g of sliced cocoons were boiled in 4 L of 0.02 M Na_2SO_3 (Acros Organics, Belgium) for 30 minutes. Subsequently, the degummed SF was washed three times in 2 L of distilled water for 20 minutes and left in a fume hood overnight to dry at room temperature (Figure 1).

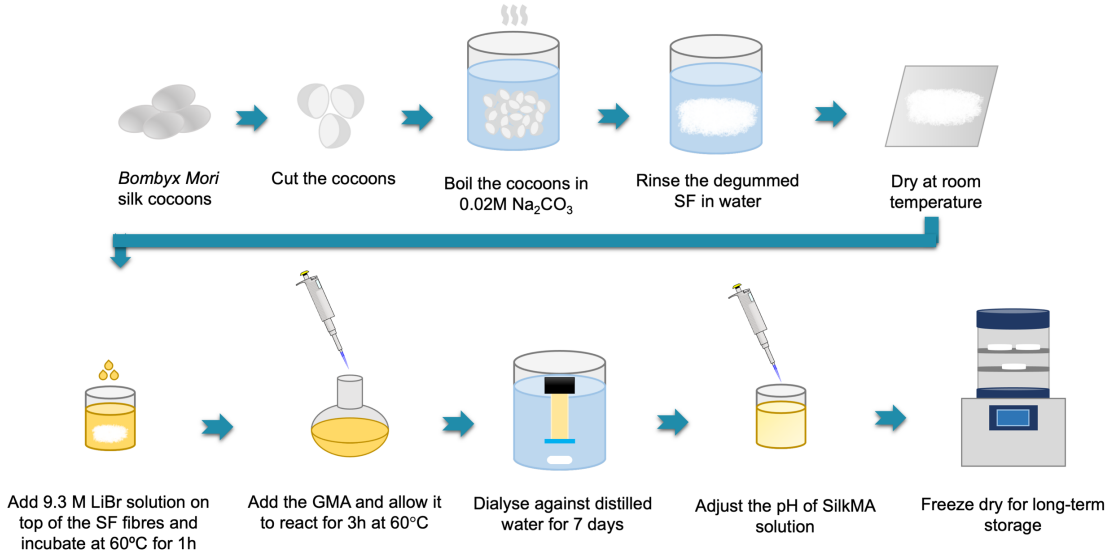

Figure 1. Workflow for SF extraction and SilkMA synthesis: degumming, dissolution in LiBr, methacrylation, dialysis and freeze-drying.

2.1.2 SilkMA Synthesis

Briefly, 25% (w/v) of degummed SF solution was prepared by pouring a 9.3 M lithium bromide solution, LiBr, (Acros Organics, Belgium) on the tightly packed degummed silk fibroin fibres. The beaker was covered with aluminium foil and transferred to an incubator at 60°C. After 1

h, the fibres were completely dissolved and the glycidyl methacrylate, GMA, (Sigma-Aldrich, USA) was added to the solution at a rate of 0.5 mL/min (10% v/v) and allowed to react for 3 h at 60°C with a stirring speed of 300 rpm. The solution was then dialysed against distilled water for 7 days at 4°C using 12-14 kDa cut-off dialysis tubes (Thermo Scientific, USA). After dialysis, the SilkMA solution was diluted to 2% (w/v) and the pH adjusted to 5, 7 or 8 using 1 mM sodium hydroxide solution (Sigma-Aldrich, USA). Lastly, SilkMA solutions were lyophilised for 2 days to generate a white porous foam, which was stored at -80°C until further use.

2.2 Degree of Methacrylation

The degree of methacrylation (DM%) was quantified by proton nuclear magnetic resonance (^{1}H-NMR). Briefly, 5 mg of SilkMA were dissolved in 600 µL deuterium oxide (Sigma-Aldrich, USA). The ^{1}H-NMR spectra of raw SF and SilkMA were recorded using a Bruker NEO NMR spectrometer fitted with a 'smart'-BBFO probe (Bruker, Austria) operating at 400 MHz for 1 hour. Spectra were recorded at 25°C using 250 scans and a delay of 12 seconds between scans. Baseline and phase correction were applied before integrating the peaks of interest with Topspin software (Bruker, Austria). The signal from the aromatic amino acids (6.9 - 7.5 ppm) was used as the internal reference to normalise the amine signals (2.83 - 3.14 ppm) [33]. As GMA is reported to react with SF through the primary amines on lysine residues, the extent of substitution was calculated by normalisation to the number of free amino groups of original SF [33]. The degree of methacrylation was calculated using the following equation:

$$\text{DM}\ (\%) = \frac{\text{lysine integration signal of SilkMA}}{\text{lysine integration signal of SF}} \times\ 100 \qquad (1)$$

2.3 Hydrogel Fabrication

SilkMA prepolymer solutions were prepared by dissolving an appropriate amount of SilkMA in distilled water at room temperature overnight. The resulting viscous solutions were filtrated using Miracloth (Merck Millipore, USA) and the final concentration was calculated. A fresh stock solution of 2% (w/v) lithium phenyl-2,4,6-trimethylbenzoylphospinate (LAP) (Sigma-Aldrich, UK) in phosphate-buffered saline, PBS pH 7.4, (Sigma-Aldrich, UK) was prepared. The photoinitiator was added to the SilkMA solution to a final concentration of 0.5% (w/v) and the resulting solution was mixed at room temperature. The hydrogel precursor solutions were photocured through UV-light using an OmniCure S1500 (Lumen Dynamics, Ontario, Canada)

with a 365 nm filter. Briefly, 200 µL of 15% (w/v) SilkMA prepolymer solution was pipetted onto a 12 mm cylindrical mould and then exposed to 3 mW/cm^2 of UV-A for 5 minutes. In this study, three different SilkMA hydrogels were prepared: SilkMA pH 5 (SF5), SilkMA pH 7 (SF7) and SilkMA pH 8 (SF8).

2.4 Transparency

Light absorbance of hydrogels in the visible range (400-800 nm) was measured using a microplate reader (Spark Multimode, Tecan, Switzerland). The measurements were conducted in triplicate using SilkMA hydrogels (diameter = 12 mm, thickness = 1.2 mm) in PBS, with pure PBS serving as a blank control. Subsequently, the transmittance was calculated using the following equation:

$$\text{Transmittance (\%)} = 10^{2-\text{Absorbance}} \quad (2)$$

2.5 Swelling Properties

Since swelling characteristics are largely dependent on the polymer chain length, cross-linking density and mesh size of the hydrogel, the same polymer batch was used to prepare all hydrogels, avoiding molecular weight and DM% variability [36],[37]. SilkMA hydrogels with a diameter of 12 mm and thickness of 1.2 mm were prepared. W_{t0}), the samples were hydrated in PBS and placed in an incubator at 37°C. After 24 $W_{swollen}$) was measured. The swelling (SR) was calculated according to the following equations:

$$\text{SR (\%)} = \frac{W_{swollen} - W_{t0}}{W_{t0}} \times 100 \quad (3)$$

The thickness of the fresh and swollen hydrogels was estimated using ImageJ software (NIH, version 2.0) and the expansion (%) in PBS after 24 hours calculated.

2.6 Rheology

The storage modulus (G') and loss modulus (G'') of freshly prepared SilkMA hydrogels were measured in oscillatory mode at 37°C using a plate-plate geometry and a 1.2 mm gap between plates (Kinexus Pro+, Malvern, UK). After running an amplitude sweep to determine the linear

viscoelastic range (LVER), a frequency sweep was conducted between 0.01-10 Hz at 0.5% shear strain.

2.7 Mechanical Characterisation

Cyclic testing was performed using an Instron 5542 mechanical tester (Instron, USA) with a 2 kN load cell. Cylindrical hydrogels (diameter = 8 mm, thickness = 2 mm) were prepared as previously described and incubated in PBS for 4 h prior to testing. The dimensions of the samples were determined using a digital caliper. Compressive tests were performed at a rate of 1 mm/min up to a maximum strain of 60% of the original height by performing 8 cycles of loading and unloading. The compressive strain (mm) and load (N) was recorded using Bluehill 3 software. The compressive moduli were calculated from the slope of the linear region on the stress (kPa) versus strain (mm/mm) curves.

2.8 Fourier Transform Infrared Spectroscopy (FTIR)

FTIR was used to assess conformational structural changes in SilkMA hydrogels prepared at pH 5, 7 or 8 after different incubation times (0, 7, 14, 21 and 28 days). Freeze-dried samples were analysed using a Nicolet iS5 spectrometer equipped with an iD5 ATR accessory (Thermo Scientific, USA). For each spectrum, 64 scans were acquired in the spectral range of 4000-550 cm^{-1} with a resolution of 4 cm^{-1}. Fourier self-deconvolution (FSD) of the infrared spectra covering the Amide I region (1595-1705 cm^{-1}) was conducted using OMNIC software (Thermo Scientific, USA). Deconvolution was automatically performed using Gaussian/Lorentzian line shape with a noise reduction factor of 0.3. The deconvoluted Amine I spectra were area normalised and single band areas used to calculate the percentage of secondary structures. The peak band assignment was based on the work of Hu et al [38].

2.9 Thioflavin T Binding Assay

Thioflavin T (ThT) (Sigma Aldrich, USA) was used to qualitatively study the β−sheet content overtime on hydrogels prepared at pH 5, 7 and 8. Briefly, the hydrogels were stained for 10 minutes in a freshly prepared 1% (w/v) ThT solution in PBS. Subsequently, the samples were rinsed with 70% (v/v) ethanol and washed three times with distilled water. A fluorescence intensity scan was performed using a microplate reader (Spark Multimode, Tecan, Switzerland) at 360 nm excitation, measuring the emission spectrum in the 400-700 nm range.

2.10 *In vitro* Cell Studies

Human Dermal Fibroblasts (HDFs - ATCC Cat. PCS-201-012; Passage number 9) were cultured in Dulbecco's modified eagle medium (DMEM - Sigma Aldrich, UK) and supplemented with 10% fetal bovine serum (Sigma Aldrich, UK), 1% penicillin/streptomycin (Sigma Aldrich, UK) and 2 mM L-glutamine (Sigma Aldrich, UK). All cultures were maintained in tissue culture treated polystyrene flasks at 37°C with 5% CO_2 in a humidified incubator and passaged at 80% confluency.

2.10.1 In vitro Cytocompatibility of Uncured SilkMA Solutions

SilkMA prepolymer solutions were UV-sterilised for 20 minutes prior to use. Tissue culture treated 24-well plates (Corning, UK) were initially seeded with HDFs (1 x 10^4 cells/well). After 24 h, DMEM media was replaced with fresh supplemented DMEM containing 20% (v/v) prepolymer solution or 20% (v/v) PBS (control group). The monolayer cultures were incubated at 37°C with 5% CO_2 in a humidified incubator and cell viability, metabolic activity and cell proliferation were assessed after 24 and 48 h.

2.10.2 In vitro Cytocompatibility of SilkMA Hydrogels

SilkMA prepolymer solutions were prepared as previously described and gelatin methacryloyl (GelMA - type A, bloom 300), a well-studied photosensitive polymer was used for comparison purposes. Briefly, 15% (w/v) GelMA prepolymer solution was prepared by dissolving an appropriate amount of polymer in PBS at 37°C for 30 minutes. SilkMA and GelMA prepolymer solutions were sterilised by exposure to germicidal UV light for 20 minutes. Then, filter-sterile LAP was added to the SilkMA and GelMA prepolymer solutions to a final concentration of 0.5% (w/v) and the resulting solutions were mixed. The SilkMA and GelMA hydrogels were photocrosslinked using 3 mW/cm^2 of UV-A for 5 minutes in 48-well suspension cell culture plates (Sarstedt, UK). After curing, the hydrogels were washed with sterile PBS (Sigma Aldrich, UK) for 15 minutes and soaked in supplemented DMEM overnight. One hour before cell seeding, the hydrogel matrices were partially dried to potentiate cell penetration. Then, 60 μL of cell suspension was added dropwise onto each hydrogel (9 x 10^3 cells per scaffold) and samples were incubated for 1 h at 37°C with 5% CO_2 to bolster cell adhesion. After 1 h, DMEM was carefully added to the wells without disturbing the cell-laden hydrogels [39]. Culture medium was changed every two days. Cell viability and metabolic activity were assessed after 2, 7 and 14 days.

2.10.2.1 Cell Viability

Cell viability was evaluated using a Live/Dead assay (Thermo Fisher, UK) following the manufacturer's protocol. Briefly, SYTO 10 green fluorescent nucleic acid stain (2 μL/mL) and ethidium homodimer-2 nucleic acid stain (2 μL/mL) were diluted in PBS to form the staining solution. At each time point, cell medium was removed, and samples were incubated with the staining solution for 15 minutes in the dark at 37°C. The staining solution was removed, and the samples were washed twice with PBS. The monolayer cultures and cell-seeded hydrogels were imaged with a fluorescent microscope (EVOS M5000, Thermo Fisher, UK) and a confocal scanning microscope (Zeiss LSM710, Carl Zeiss, Germany), respectively.

2.10.2.2 Metabolic Activity

AlamarBlue™ assay (Thermo Fisher, UK) was used to determinate the relative metabolic activity according to the manufacturer's protocol. Briefly, the samples were incubated with 0.5 mL of 10% alamarBlue™ reagent in culture medium for 4 h at 37°C with 5% CO_2. Thereafter, 50 μL of cell culture medium were transferred to a 96-well plate (Corning, UK) and the fluorescence intensity was measured with a microplate reader (Spark Multimode, Tecan, Switzerland) using an excitation wavelength of 540 nm and an emission wavelength of 590 nm. Acellular hydrogels were used as a negative control and their fluorescence was subtracted from the same group seeded hydrogels to account for the background ($n \geq 4$).

2.10.2.3 Cell Proliferation

DNA content was quantified using the Quant-iT PicoGreen DNA assay (Invitrogen, Life Technologies, UK). Briefly, cells were lysed in 0.1% Triton™ X-100 in PBS (Sigma-Aldrich, UK) and kept at -80°C until further analysis. Cells were lysed following three freeze/thaw cycles between –80°C and 37°C with vortexing. After spinning down the samples at 300 g for 5 min to remove non-genomic material, 10 μL of cell lysate was added to 90 μL of TE (10mM Tris-HCl, 1 mM EDTA) buffer in a 96-well plate (Corning, UK). 100 μL of PicoGreen reagent was added to all samples and then incubated for 5 min. The fluorescence intensity was then measured with a microplate reader (Spark Multimode, Tecan, Switzerland) at an excitation and emission wavelength of 480 and 520 nm, respectively.

2.11 Statistical Analysis

For each experiment, at least three samples were tested. One or two-way analysis of variance (ANOVA) and the Tukey test were used to determine statistically significant differences with

GraphPad Prism 8.0 software. The level of significance was set at $p<0.05$. Data are presented as mean value ± standard deviation (SD). Samples were tested in triplicate for each condition.

3. Results

3.1 Physicochemical Characterisation of SilkMA Gels

^{1}H-NMR spectroscopy was used to confirm the methacrylate-functionalization of SF (Figure 2). The appearance of the characteristic resonances of the methacrylate vinyl group (olefinic hydrogen, δ = 6.2 ppm) and methyl group (methyl hydrogen, δ = 1.8 ppm) of GMA confirmed the covalent functionalization of SF with methacrylate groups whilst the absence of epoxide ring group (aliphatic protons, δ = 2.82 and 2.67 ppm) indicates the complete removal of unreacted GMA through dialysis [33], [40]. The decrease in the lysine methylene signal (δ = 3 ppm) indicated that the DM% was 35-40% after 3h reaction with 10% (v/v) GMA. In this work, three different hydrogel formulations were prepared: SilkMA pH 5 (SF5), SilkMA pH 7 (SF7) and SilkMA pH 8 (SF8).

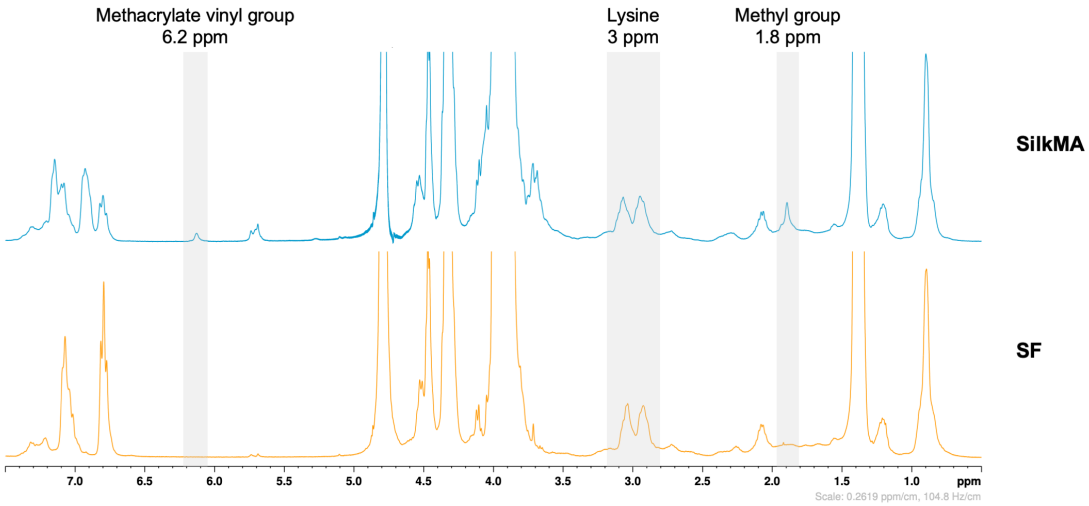

Figure 2 - ^{1}H-NMR spectra of SilkMA (top) and raw SF (bottom). The presence of the methacrylate vinyl group signal (δ = 6.2 ppm) and methyl group signal (δ = 1.8 ppm) after removal of unreacted GMA by dialysis confirmed the covalent functionalisation of SF with methacrylate groups.

Transmittance profiles of 15% (w/v) SilkMA hydrogels in the visible light range are shown in **Figure 3**a. In general, all SilkMA hydrogels displayed high optical clarity, with transmittance values ranging from 82.1 ± 3.0% to 91.6 ± 0.9% (**Figure 3**b and c). The SilkMA hydrogels exhibited enhanced transparency in the visible range with increasing pH, with the SF8 hydrogel eliciting a statistically significant increase in transparency compared to the SF5 hydrogels (10.4 ± 2.3%, $p<0.01$) (**Figure 3**b).

To determine the swelling (SR), water uptake (q) and expansion, SF5, SF7 and SF8 hydrogels were incubated in PBS buffer at 37°C for 24 h. The swelling characteristics were directly proportional to the hydrogel pH; the SR of SF5, SF7 and SF8 was 39.3 ± 3.7%, 80.9 ± 11.9% and 86.2 ± 7.9%, respectively, with SF 7 ($p<0.001$) and SF8 ($p<0.0001$) exhibiting a two-fold significant increased compared to SF5 (**Figure 3**d). As shown in **Figure 3**e, the expansion of SilkMA hydrogels in PBS is not statistically significant between groups, despite ranging from 13.0 ± 7.0% to 34.4 ± 13.9% for SF5 and SF8, respectively.

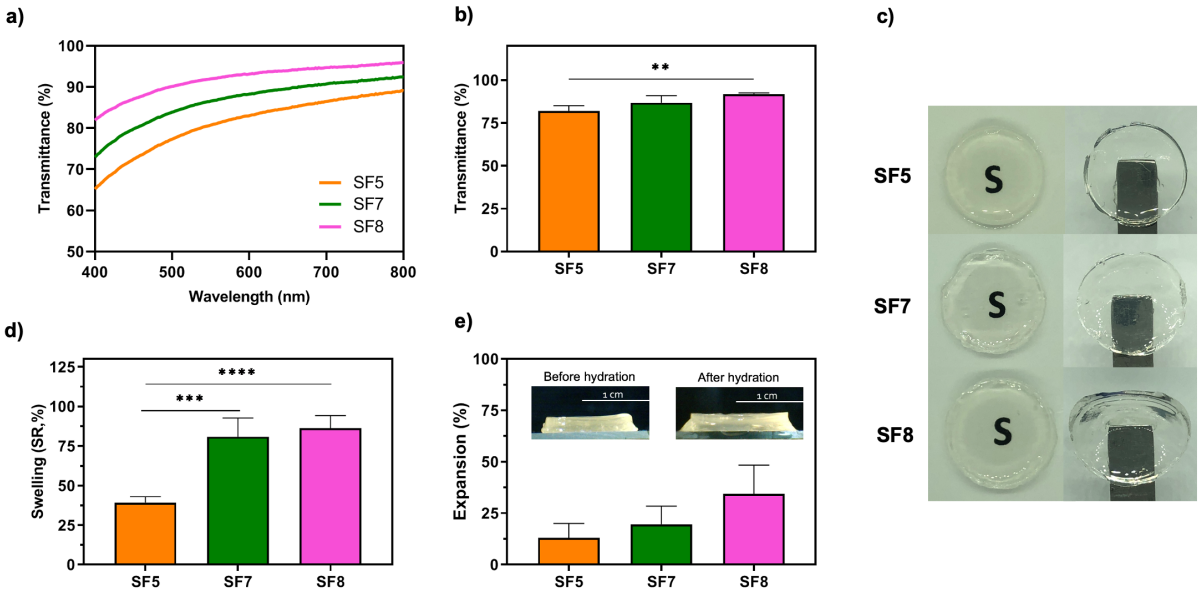

Figure 3. SilkMA hydrogels transmittance in the visible range: a) transmittance profiles, b) average optical transmittance and c) optical clarity and rigidity of SilkMA hydrogels. (%). Swelling properties of SilkMA hydrogels in PBS at 37°C: d) swelling (%) and e) hydrogel expansion (%). Hydrogel diameter = 12 mm. Data presented as mean value ± SD (*$p<0.05$, **$p<0.01$, ***$p<0.001$, ****$p<0.0001$).

The viscoelastic properties of the SilkMA hydrogels were investigated via rheometry. The storage modulus (G') represents the instantaneous, elastic and reversible response of a material to stretching and deformation of chemical bonds, while the loss modulus (G'') represents the time-dependent, viscous response and irreversible rearrangement of the internal polymeric structure of the material [41]. Firstly, the LVER was determined by varying the strain at a constant frequency. Up to 1% strain, all groups were structurally stable with constant values for G' and G'' (data not shown). Then, G' and G'' values of the hydrogels were recorded as a function of frequency (0.01-10 Hz, 0.5% strain) at 37°C. As shown in **Figure 4**a, limited changes were observed in the storage modulus G' in the frequency range studied, confirming the high stability of the hydrogels. Moreover, G'' is an order of magnitude lower than G', which is typical behaviour of viscoelastic materials (**Figure 4**c). Importantly, our results indicate that

decreasing the pH of the prepolymer solution resulted in significantly stiffer hydrogels; SF5 hydrogels had a storage modulus significantly greater than SF7 ($p<0.0001$) and SF8 ($p<0.0001$) hydrogels by 3 and 6-fold, respectively (**Figure 4**b). The differences in stiffness were noticeable when handling the hydrogels, with SF8 hydrogels being substantially more difficult to handle (**Figure 4c**). Finally, the damping factor (tan δ = G''/G') was greater for SF 7 and SF8 but lower than 0.08 for all groups, suggesting that all SilkMA hydrogels behaved as elastomeric materials (**Figure 4**d) [33], [42].

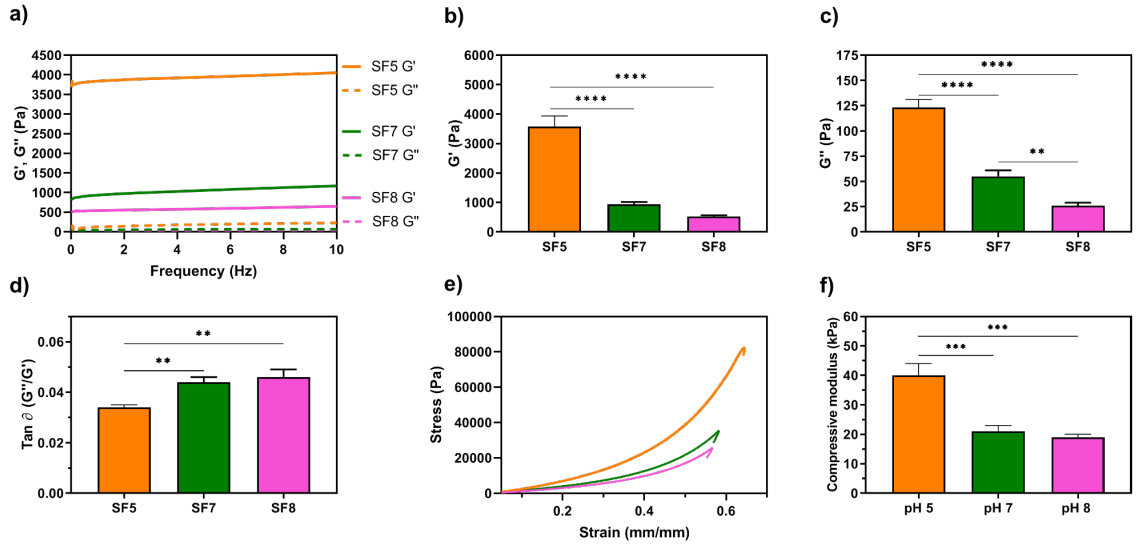

Figure 4. Rheological properties of SilkMA hydrogels: a) representative frequency sweep, b) storage modulus (G'), c) loss modulus (G'') and d) damping factor (tan δ). Cyclic compressive mechanical testing of SilkMA hydrogels: e) representative compressive strain-stress curves and f) compressive moduli. Data presented as mean value ± SD (*p<0.05, **p<0.01, ***p< 0.001, ****p<0.0001).

The mechanical properties of SilkMA hydrogels were determined through compression testing. Our results revealed that all groups were mechanical stable for cyclic compressive mechanical testing (**Figure 4**e). In agreement with the rheology data, statistical analysis illustrated a significant pH effect on the compressive modulus of SilkMA hydrogels with SF5 hydrogels showcasing a significantly higher compressive modulus than SF7 and SF8 ($p<0.001$). Specifically, the compressive modulus is 21 ± 2 kPa for SF7 and 40 ± 4 kPa for SF5, a 2-fold increase (**Figure 4**f).

3.2 Natural conformational changes in SilkMA hydrogels over time

SF materials are reported to suffer spontaneous conformational changes at physiological conditions [3], [5], [43], [44]. To further understand the observed differences in the properties

of SilkMA gels, the secondary structure of the hydrogels was studied using Fourier transform infrared spectroscopy (FTIR) and a thioflavin T binding assay (**Figure 5**). As shown in **Figure 5**a, the major bands of the protein infrared spectrum can be observed in SilkMA hydrogels: the amide I (1700-1600 cm^{-1}), amide II (1600-1500 cm^{-1}) and amide III (1350-1200 cm^{-1}) [45]. At day 0, the main absorption bands were observed at 1643 cm^{-1} (amide I) and 1525 cm^{-1} (amide II), which are characteristic of the random coil conformation. However, after incubating the hydrogels for 28 days at physiological conditions, these absorption bands shifted to 1629 cm^{-1} (amide I) and 1512 cm^{-1} (amide II), suggesting an increase in the β-sheet content [45]. Importantly, the amide I (1700-1600 cm^{-1}) region is very sensitive to the secondary structure and can be deconvoluted into discreet component bands indicative of tyrosine side chains, random coil, turns, α-helixes and β-sheet structures [46],[45]. Deconvoluted amine I spectra were area normalized and the areas of the single bands were used to calculate the relative content of secondary structures, as shown in Table 1.

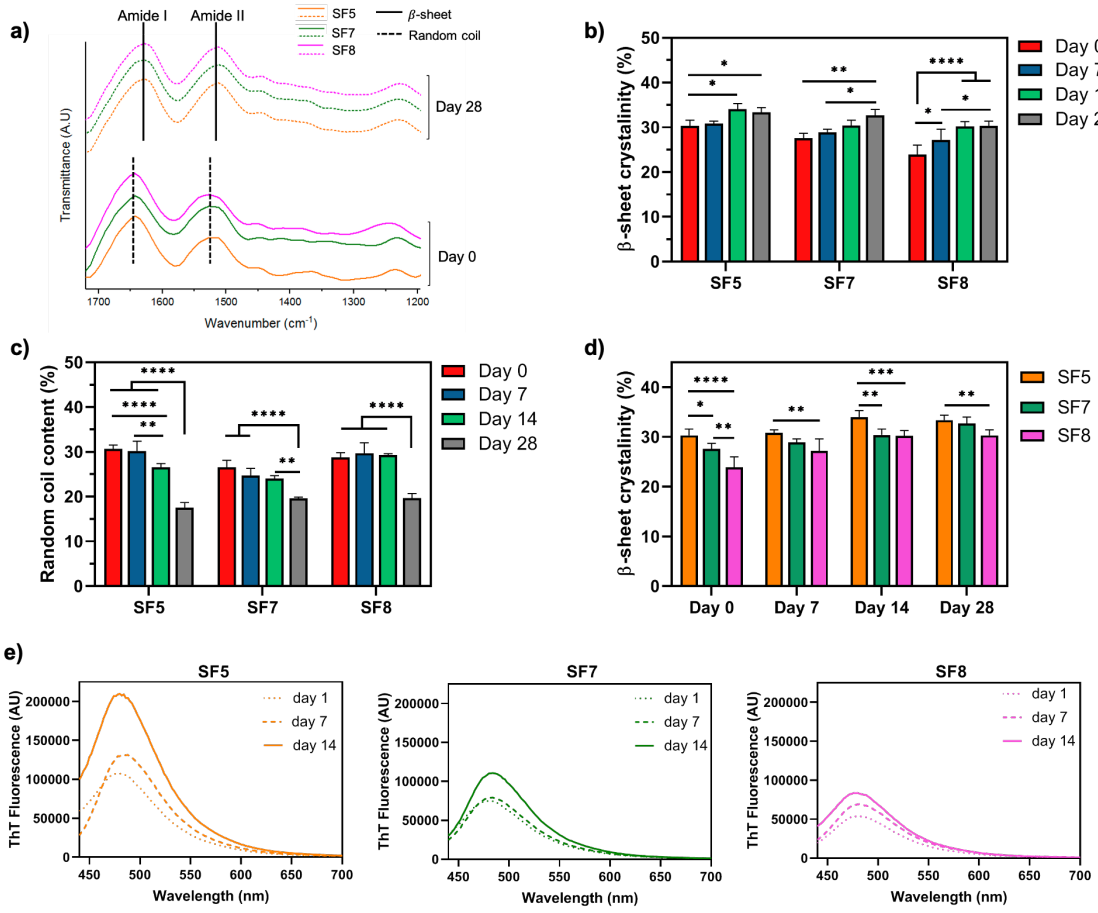

Figure 5. Study of conformational transitions on SilkMA hydrogels over time: a) FTIR spectra of SilkMA hydrogels after crosslinking (day 0) and 28 days after incubation at physiological conditions, b) β-sheet crystallinity content over time (day 0, 7, 14 and 28), c) random coil content over time (day 0, 7, 14 and 28) and

d) comparison of β-sheet content between groups at different time points (day 0, 7, 14 and 28). e) Thioflavin T staining of SilkMA hydrogels at 1, 7, and 14 days. Emission spectrum in the 440-700 nm range under 360 nm excitation. Data presented as mean value ± SD (*p<0.05, **p<0.01, ***p<0.001, ****p<0.0001).

An increase in β-sheet content was accompanied by a decrease in the random coil content upon ageing for all groups studied (**Figure 5**b and c). Moreover, the β-sheet crystallinity was shown to be inversely proportional to SilkMA hydrogel pH (**Figure 5**d). The β-sheet content was significantly different between the groups at day 0, corresponding to 30.3 ± 1.3%, 27.6 ± 1.1% and 23.9 ± 2.1% for SF5, SF 7 and SF 8, respectively. In contrast, after 28 days of incubation and although the β-sheet crystallinity in SF5 is greater than in SF7 and SF8, the difference is only statistically significant for the latter ($p<0.01$).

Table 1. Relative content of secondary structures in SilkMA hydrogels incubated at 37ºC for 0, 7, 14 and 28 days. Data obtained from deconvolution of the infrared spectra covering the amide I region. Data presented as mean value ± SD (n=4).

SilkMA sample	Time (days)	Side Chains (%)	Turns (%)	Random coil (%)	α-helices (%)	β-sheet (%)
SF5	0	5 ± 0.4	23.6 ± 0.8	30.7 ± 0.8	10.5 ± 0.3	30.3 ± 1.3
	7	12.3 ± 3.3	16.2 ± 0.5	30.2 ± 2.2	10.5 ± 4.0	30.8 ± 0.6
	14	12.6 ± 0.8	18.8 ± 0.4	26.6 ± 0.8	8.0 ± 1.5	34.0 ± 1.3
	28	19.9 ± 2.1	22.5 ± 1.4	17.5 ± 1.2	6.8 ± 0.3	33.4 ± 1.0
SF7	0	14.6 ± 1.2	21.1 ± 0.4	26.6 ± 1.5	10.2 ± 0.4	27.6 ± 1.1
	7	16.0 ± 1.8	21.1 ± 0.9	24.7 ± 1.6	9.3 ± 0.4	28.9 ± 0.7
	14	15.6 ± 0.5	20.4 ± 1.9	24.0 ± 0.7	9.5 ± 0.5	30.4 ± 1.2
	28	24.5 ± 1.2	16.1 ± 0.6	19.6 ± 0.3	7.1 ± 0.6	32.7 ± 1.3
SF8	0	14.7 ± 1.4	22.5 ± 1.4	28.8 ± 1.0	10.1 ± 0.3	23.9 ± 2.1
	7	12.5 ± 4.2	19.1 ± 3.5	29.7 ± 2.3	11.5 ± 1.0	27.2 ± 2.4
	14	14.1 ± 0.4	15.6 ± 1.7	29.3 ± 0.3	10.8 ± 0.7	30.2 ± 1.1
	28	27.7 ± 1.7	15.4 ± 2.5	19.7 ± 1.0	7.0 ± 0.1	30.3 ± 1.1

Thioflavin T (ThT) is a powerful fluorescent marker to identify β-aggregates, such as β-amyloid and β-sheet [37], [47]. Herein, this staining approach was used to qualitatively confirm time-dependent conformational changes assessed by FTIR. Since the intensity is proportional to the sample mass, the hydrogels were prepared with the same volume of prepolymer solution. However, different degradation profiles might have interfered with the intensities obtained at

day 7 and 14. The emission spectra of SilkMA hydrogels at day 1, 7 and 14 can be observed in **Figure 5**e. Our results show that fluorescence intensity increased with time for all groups studied. Moreover, the fluorescence intensity is inversely proportional to the hydrogel pH, in agreement with the FTIR deconvolution data. When comparing the results at day 1, the maximum ThT fluorescence for SF5 (107000 AU) was higher than SF7 (75000 AU) and SF8 (54000 AU) hydrogels. Similarly, after 14 days SF5 maximum intensity (210000 AU) was 2 and 2.2-fold higher than SF7 (110000 AU) and SF8 (94000 AU).

To further analyse the effect of the spontaneous conformational transitions on the physical and mechanical properties of SilkMA hydrogels, the optical transmittance and compressive modulus were determined at different incubation time points (**Figure 6**). The obtained results show that the optical transparency of SilkMA hydrogels is directly proportional to the prepolymer solution pH and decreases over time, as the hydrogel crystallinity increases. As previously mentioned, the transmittance of SilkMA hydrogels at day 0 was between 82.1 ± 3.0% and 91.6 ± 0.9%, for SF5 and SF8 hydrogels ($p<0.01$), respectively (**Figure 6**a). Despite this 9.5% difference, all samples were initially transparent to the naked eye (**Figure 6**b). After 7 days, SF5 hydrogels had the highest decrease in transparency (12.1%) to 71.8 ± 2.3%, while SF8 hydrogels exhibited a reduction of 0.9% to 89.9 ± 1.4%, with the SF5 group displaying a significant reduction in transparency when compared to the SF7 ($p<0.001$) and SF8 ($p<0.0001$) gels. At day 14, the optical properties of SF5 and SF7 hydrogels were not statistically different, however, SF8 hydrogels had a transmittance of 85.1 ± 4.9%, which is higher than the transmittance of SF5 hydrogels at day 0 (83.9 ± 3.7%). After 28 days of incubation, the optical transmittance of all SilkMA groups decreased to values of approximately 50% (Figure 5a and b). Finally, the mechanical toughening impact of the increasing β-sheet content on the hydrogels was studied by cyclic compressive testing. The hydrogel stiffness consistently increased over time driven by the higher β-sheet crystallinity. The compressive modulus rose by 2 orders of magnitude for SF5 (from 40 kPa to 1.1 MPa) and 1 order of magnitude for SF7 (from 21 kPa to 870 kPa) and SF8 (from 19 kPa to 631 kPa) within 14 days (Figure 6c). The difference between day 0 and day 7 was not statistically significant for SF7 and SF8 samples, however, at day 7, SF5 showed a compressive modulus 25 and 81-fold superior to SF7 ($p<0.001$) and SF8 ($p<0.0001$), respectively (Figure 6d). After 14 days, the compressive modulus ranged from 631 kPa to 1.1 MPa, being statistically different between all groups (Figure 6e).

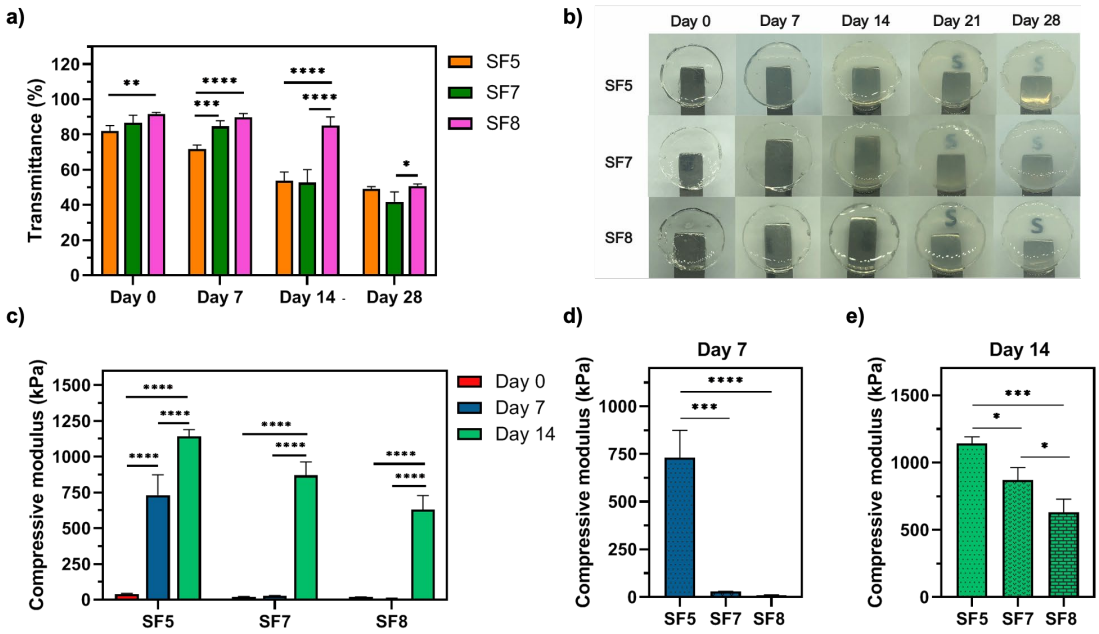

Figure 6. Study of the natural conformational changes in SilkMA hydrogels incubated in PBS at 37°C. a) Average optical transmittance in the visible range of SilkMA hydrogels at 0, 7, 14, and 28 days. b) Appearance of SilkMA hydrogels after incubation for 0, 7, 14, 21 and 28 days (hydrogel diameter = 1 cm). c) Mechanical toughening impact of the increasing β-sheet content on SilkMA hydrogels. d) Compression moduli of SilkMA hydrogels after incubating for 7 days. e) Compression moduli of SilkMA hydrogels after incubating for 14 days. Data presented as mean value ± standard deviation (*p<0.05, **p<0.01, ***p<0.001, ****p<0.0001).

3.3 In vitro Assessment of Cytocompatibility

The cytotoxicity of uncrosslinked SilkMA prepolymer solutions was studied by using HDF cells seeded on tissue culture well-plates and compared with cells cultured in complete media. Fluorescence staining (**Figure 7**a) indicate high cell viability (>90%) for all tested conditions, suggesting that SilkMA prepolymer solutions did not induce cytotoxicity. Variations in cell metabolism and proliferation were not statistically different between SilkMA samples throughout the experiment, with a time-dependant increase observed in both groups. However, the controls showed higher metabolic activity than SF5 ($p<0.0001$) and SF7 ($p<0.0001$) (**Figure 7**b). DNA content results were in agreement with the metabolic activity, with controls showing higher DNA concentration compared to SF5 ($p<0.01$) and SF7 ($p<0.001$) 48 h post seeding (**Figure 7**c).

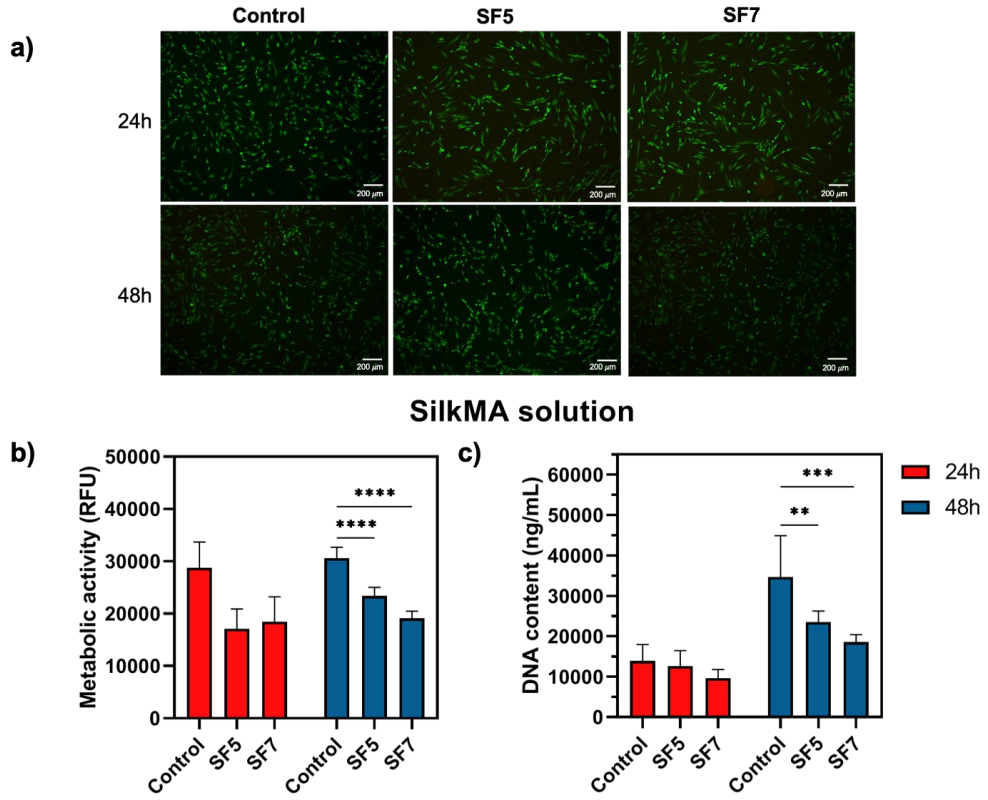

Figure 7. Cytotoxicity of uncrosslinked SilkMA prepolymer solutions. a) Live/Dead images of HDFs seeded on tissue culture well-plates with media (control) and media supplemented with SF5 and SF7 prepolymer solutions. Scale bar = 200 μm. b) Quantification of the metabolic activity by AlamarBlue assay 24h and 48h after cell seeding. c) Quantification of cell proliferation by Picogreen DNA assay 24h and 48h after cell seeding. Data presented as mean value ± SD (*p<0.05, **p<0.01, ***p< 0.001, ****p<0.0001).

The ability of SilkMA hydrogels to support cell attachment and proliferation was evaluated by direct seeding of HDF cells on SF5 and SF7 hydrogels and compared with GelMA, an extensively studied hydrogel for 3D cells culture applications [48]. Cell viability, metabolic activity and proliferation were assessed 2, 7 and 14 days post seeding. As shown in Figure 8a, Live/Dead staining showed that SilkMA hydrogels are capable of supporting cell attachment and proliferation for up to 14 days. 2 days after seeding, most cells deposited on SilkMA hydrogels exhibited a rounded morphology with limited spreading, whereas cells on GelMA hydrogels actively spread, showing a spindle-shaped morphology characteristic of HDFs. This effect is in line with available literature as previous reports indicate that SF from *B.mori* has limited initial cellular response as a result from limited adhesive amino acid sequences (e.g. RGD) on its composition [42][49]. However, 7 days post-seeding the cells exhibited a typical fibroblastic morphology and proliferated to reach confluence on the SilkMA gels, similar to that observed on GelMA hydrogels. After 14 days, some dead cells can be observed in all

groups due to over confluency. This limited initial interaction for the SilkMA hydrogels is further observed in the metabolic activity measurements which is likely to be influenced by cell adhesion. Cell metabolism was significantly ($p<0.0001$) higher on GelMA hydrogels at each time point (Figure 8b). However, despite both SilkMA groups showing a significantly lower metabolic activity than GelMA at day 7, specifically 46% (SF5, $p<0.0001$) and 39% (SF7, $p<0.0001$), this difference decreases to approximately 19% for both groups ($p<0.0001$) after 14 days (Figure 8b). The metabolic activity of cells seeded on SF5 and SF7 was not statistically different at each time point assessed, with a time-dependant increase in metabolic activity observed in both groups.

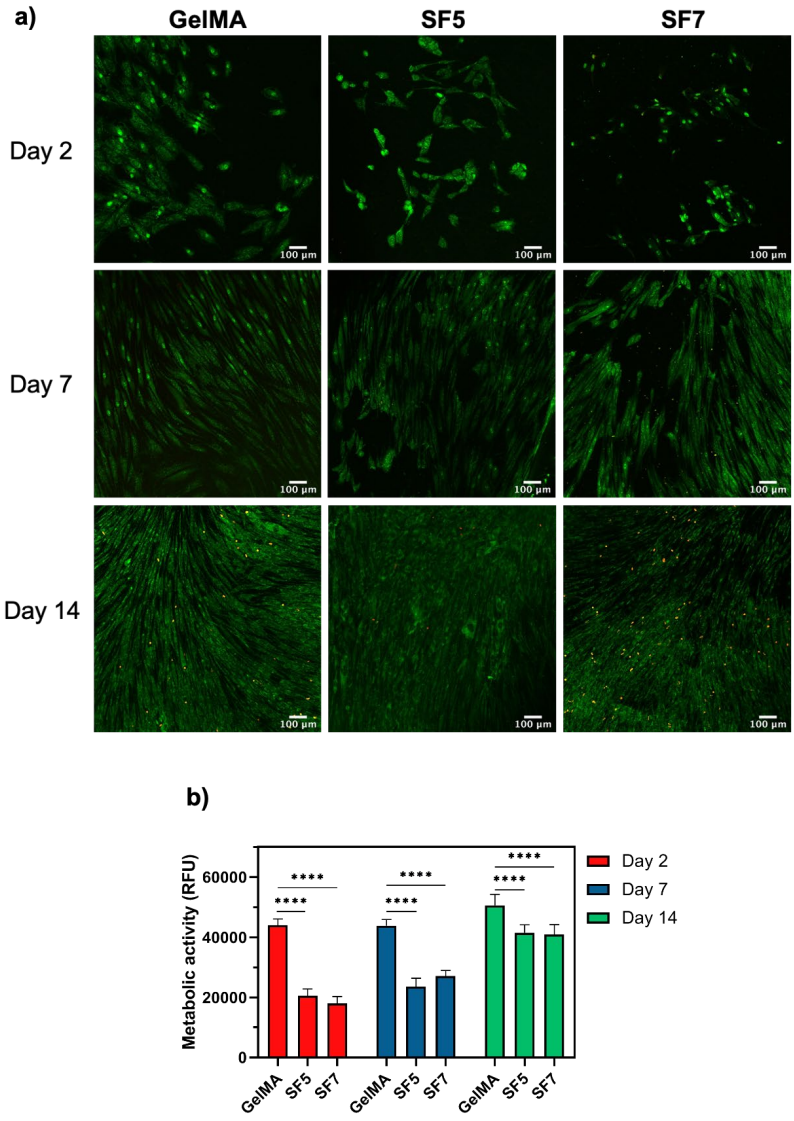

Figure 8. Cytotoxicity of SilkMA prepolymer hydrogels: a) Live/Dead images of HDFs seeded on GelMA, SF5 and SF7 hydrogels. b) Quantification of the metabolic activity by alamarBlue assay 2, 7 and 14 days after cell seeding. Data presented as mean value ± SD (*$p<0.05$, **$p<0.01$, ***$p<0.001$, ****$p<0.0001$).

4. Discussion

Over the last decade efforts to develop chemically crosslinked SF hydrogels have been made [3], [26]. Herein, we developed a glycidyl-methacrylate-modified SF solution that can be chemically crosslinked within a few minutes using light. Cells can be encapsulated within the hydrogels by gentle mixing with the prepolymer solution before crosslinking. Several natural and synthetic polymers such as gelatin, collagen or hyaluronic acid have been previously methacrylated [50], [51], [52]. Vinyl-containing monomers, such as glycidyl methacrylate and methacrylic anhydride are commonly used to methacrylate proteins. After dialysis, the purified methacrylated-protein solution has a pH between 4.5-5.5, contrasting with the neutral pH of pure silk solutions. Considering the role of pH in the molecular aggregation of SF proteins *in vivo,* we hypothesise that the pH of the prepolymer solution will play a determinant role in the short and long-term properties of SilkMA hydrogels, being essential to control function and ensure reproducible manufacturing.

To study the impact of the prepolymer solution pH on the properties of SilkMA gels, three different formulations were prepared: SilkMA pH 5 (SF5), SilkMA pH 7 (SF7) and SilkMA pH 8 (SF8). In general, all SilkMA hydrogels presented high transparency, elasticity and were easy to handle (**Figure 3**c). Despite perceptible differences in rigidity, all SilkMA gels behaved as viscoelastic solids, as demonstrated by the higher G' for all groups studied (**Figure 4**a). When freshly prepared hydrogels were studied, we found that SF5 hydrogels exhibited significantly greater storage and compressive modulus than SF7 and SF8 hydrogels (**Figure 4**b and f).

To further understand the observed differences in the properties of SilkMA gels, the secondary structure of the gels was investigated using FTIR. Since the amide I region of the spectra is very sensitive to the secondary structure, it can be deconvoluted using a Fourier self-deconvolution algorithm to determine the relative contribution of each structure fraction [46],[45]. As shown in Table 1, our results show a time-dependent reduction in the random coil content, accompanied by a β-sheet content rise for all groups. The conformational changes assessed by FTIR were qualitatively confirmed using thioflavin T staining, a fluorescent marker that binds β-sheet structures (**Figure 5**e). Time-dependent conformational transitions are expected in silk-based materials and have been previously reported by other authors [3], [5], [44], [53], [54].

As described by Burke et. al., the hydrogen bonding between adjacent β-sheet (physical crosslinking) is responsible for the aqueous insolubility and remarkable mechanical properties of SF [55]. In this work, the mechanical toughening impact of the β-sheet crystallinity was studied by compressive mechanical testing. As shown in **Figure 6**c, the hydrogel stiffness consistently increased over time for all studied groups, in agreement with the FTIR data. Remarkably, the compressive modulus of SF5 hydrogels, increased by 2 orders of magnitude in 14 days, while SF7 and SF8 gels increased by an order of magnitude. Typically, one of the strategies used enhance the mechanical strength of gels is by increasing the polymer concentration, however, it may negatively impact cell viability and proliferation within the scaffold as reported in the literature [56], [57]. Herein, we demonstrated that by adjusting the pH of the prepolymer solution, SilkMA hydrogel stiffness can be tailored without changing the polymer concentration or the molecular weight. Despite improving the compressive modulus, which might be advantageous for certain applications, the increase in crystallinity has a negative impact on elasticity. As shown in **Figure 3**b and c, both the optical transparency and the swelling characteristics were shown to be significantly lower for SF5 gels.

Swelling properties are critical for tissue engineering applications since a material's water content influences the transport of oxygen, nutrients and metabolites, as well as the viability and proliferation of cells [58]. As shown in **Figure 3**d, SF5 has enhanced structural stability against swelling, with a significantly lower SR than SF 7 and SF8 ($p<0.001$ and $p<0.0001$, respectively). A decrease in the network swellability is expected with an increase in the hydrophobic β-sheet content [59]. On day 0, the β-sheet content was shown to be significantly different between samples, with SF5 having on average 6.4% and 2.7% higher crystallinity than SF7 and SF8, respectively (Table 1, **Figure 5**d). Moreover, swelling can have an impact on the overall shape of a material, which must be retained *in vivo* [33]. These materials should have a minimal volume change thereby reducing the risk of implant mismatch and imparting additional stress on the surrounding tissues [60]. Thus, the dimensional stability of *in situ* crosslinked hydrogels is of critical importance. All experimental groups retained their shape and were easily handled in the swollen state. Although hydrogel expansion was not statistically significant between experimental groups, the volume increase seems to be proportional to the hydrogel pH, in agreement with the swelling characteristics (**Figure 3**f).

One of the outstanding properties of SF hydrogels is the high optical transparency in the visible range. This property is of utmost importance for many applications in tissue engineering, such as corneal substitutes and ocular adhesives [39], [61], [62]. In this work, we have quantified hydrogel transparency over time for the different studied groups. As shown in Figure 6a**,** the transparency of SF hydrogels progressively decreased after curing. Remarkably, SF8 remained optically clear after 14 days of incubation (transmittance > 85%) while SF5 and SF7 gels became opaque, transmittance ≈ 53% (Figure 6b). It has been previously reported that SF-based hydrogels become increasingly opaque over time, as the main protein conformation changes from random coil to the β-sheet crystalline form [3][37][44]. It is important to note that crystallinity is not the only factor determining the transparency of hydrogels since amorphous materials can still be opaque [37]. Since all SilkMA hydrogels were prepared at the same concentration, the ratio of polymeric network/water phase is the same. However, as shown in **Figure 3**d, the swelling characteristics are statistically different between the samples. The higher water content in SF7 and SF8 hydrogels might also play a role in the increased optical clarity.

Due to the short photocrosslinking times and mild environmental conditions, SilkMA hydrogels can be used to deliver cells. However, SF is reported to lack cell binding sequences necessary for cellular adhesion and proliferation [42][49]. In this study, the cytocompatibility of uncrosslinked SilkMA prepolymer solutions and SilkMA hydrogels was assessed *in vitro.* As shown in **Figure 7**, SilkMA prepolymer solutions did not induce cytotoxicity despite the significantly lower metabolic activity and proliferation in comparison with the control. HDF adhesion to SF5 and SF7 hydrogels was compared with GelMA, a material which provides cells with an optimal biological environment such as adhesion sequences [48]. As shown in Figure 8a, SilkMA hydrogels exhibited low toxicity although the hydrogels showed a delayed attachment and lower metabolic activity relative to the control. Despite the previously mentioned differences in stiffness and hydrophilicity, the metabolic activity of HDFs on SF5 and SF7 gels was not statistically significant. In summary, the pH of the gels did not affect cytocompatibility. Importantly, our findings showed that the seeded HDFs were able to spread and proliferate on the SilkMA hydrogels, similar to the observations on the GelMA control. The cytocompatibility of SilkMA hydrogels confirmed that SF is a promising material for tissue engineering. In the future, it would be interesting to evaluate the impact of pH-induced scaffold properties on the behaviour of cells more sensitive to environmental stimuli (e.g. stem

cells). This would provide a greater understanding of the effects of pH control on the mechanotransductive properties of the SilkMA hydrogels.

5. Conclusions

The present work studies the effect of prepolymer solution pH on the initial and long-term properties of SilkMA hydrogels. We have demonstrated, 1) the pH of prepolymer solution can be effectively used to control SilkMA conformational structure development towards utility and function, and 2) strict pH control is necessary to ensure reproducibility as physical crosslinking influences the hydrogel properties independently of the parameters controlling the chemical crosslinking reaction (e.g. DM%, polymer/photoinitiator concentration, etc). Furthermore, we developed injectable, highly elastic and transparent SilkMA hydrogels that can be photocrosslinked within minutes. These gels are suitable for cell encapsulation and displayed adequate physicochemical properties for tissue engineering applications. In the future, we believe SilkMA has the potential to be applied in the design of bioinks and bioresins.

Acknowledgments

The authors would like to sincerely thank Dr. Salvador D. Aznar-Cervantes and Dr. José L. Cenis for their help with silk fibroin extraction processes and Dr. Cécile Le Duff for her assistance with ^{1}H-NMR spectroscopy.

Funding Sources

This research did not receive any specific grant from funding agencies in the public, commercial, or not-for-profit sectors.

Data availability statement

The raw/processed data required to reproduce these findings cannot be shared at this time due to technical or time limitations.

[1] C. C. Piras and D. K. Smith, “Multicomponent polysaccharide alginate-based bioinks,” 2020.

[2] M. Sun, X. Sun, Z. Wang, S. Guo, G. Yu, and H. Yang, “Synthesis and properties of gelatin methacryloyl (GelMA) hydrogels and their recent applications in load-bearing tissue,” *Polymers (Basel).*, vol. 10, no. 11, 2018.

[3] L. P. Yan *et al.*, “Tumor Growth Suppression Induced by Biomimetic Silk Fibroin Hydrogels,” *Sci. Rep.*, vol. 6, no. January, pp. 1–11, 2016.

[4] A. P. Tabatabai, D. L. Kaplan, and D. L. Blair, “Rheology of reconstituted silk fibroin protein gels: The epitome of extreme mechanics,” *Soft Matter*, vol. 11, no. 4, pp. 756–761, 2015.

[5] J. B. Costa, J. Silva-Correia, J. M. Oliveira, and R. L. Reis, “Fast Setting Silk Fibroin Bioink for Bioprinting of Patient-Specific Memory-Shape Implants,” *Adv. Healthc. Mater.*, vol. 6, no. 22, pp. 1–8, 2017.

[6] Y. Qi *et al.*, “A review of structure construction of silk fibroin biomaterials from single structures to multi-level structures,” *Int. J. Mol. Sci.*, vol. 18, no. 3, 2017.

[7] U. J. Kim, J. Park, C. Li, H. J. Jin, R. Valluzzi, and D. L. Kaplan, “Structure and properties of silk hydrogels,” *Biomacromolecules*, vol. 5, no. 3, pp. 786–792, 2004.

[8] A. Matsumoto *et al.*, “Mechanisms of Silk Fibroin Sol - Gel Transitions,” pp. 21630–21638, 2006.

[9] L. S. Wray *et al.*, “Effect of processing on silk-based biomaterials: Reproducibility and biocompatibility,” *J. Biomed. Mater. Res. - Part B Appl. Biomater.*, vol. 99 B, no. 1, pp. 89–101, 2011.

[10] B. Kundu *et al.*, “Silk proteins for biomedical applications: Bioengineering perspectives,” *Prog. Polym. Sci.*, vol. 39, no. 2, pp. 251–267, 2014.

[11] C. W. P. Foo, E. Bini, J. Hensman, D. P. Knight, R. V. Lewis, and D. L. Kaplan, “Role of pH and charge on silk protein assembly in insects and spiders,” *Appl. Phys. A Mater. Sci. Process.*, vol. 82, no. 2, pp. 223–233, 2006.

[12] A. E. Terry, D. P. Knight, D. Porter, and F. Vollrath, “pH induced changes in the rheology of silk fibroin solution from the middle division of Bombyx mori silkworm,” *Biomacromolecules*, vol. 5, no. 3, pp. 768–772, 2004.

[13] M. Fini *et al.*, “The healing of confined critical size cancellous defects in the presence of silk fibroin hydrogel,” *Biomaterials*, vol. 26, no. 17, pp. 3527–3536, 2005.

[14] S. Nagarkar, T. Nicolai, C. Chassenieux, and A. Lele, “Structure and gelation mechanism of silk hydrogels,” *Phys. Chem. Chem. Phys.*, vol. 12, no. 15, p. 3834, 2010.

[15] K. Luo, Y. Yang, and Z. Shao, “Physically Crosslinked Biocompatible Silk-Fibroin-Based Hydrogels with High Mechanical Performance,” *Adv. Funct. Mater.*, vol. 26, no. 6, pp. 872–880, 2016.

[16] T. Dong *et al.*, “The regenerated silk fibroin hydrogel with designed architecture bioprinted by its microhydrogel,” *J. Mater. Chem. B*, vol. 7, no. 27, pp. 4328–4337,

2019.

[17] S. Hofmann *et al.*, “Silk fibroin as an organic polymer for controlled drug delivery,” *J. Control. Release*, vol. 111, no. 1–2, pp. 219–227, 2006.

[18] E. S. Gil, R. J. Spontak, and S. M. Hudson, “Effect of β-sheet crystals on the thermal and rheological behavior of protein-based hydrogels derived from gelatin and silk fibroin,” *Macromol. Biosci.*, vol. 5, no. 8, pp. 702–709, 2005.

[19] A. Alessandrino, B. Marelli, C. Arosio, S. Fare, M. C. Tanzi, and G. Freddi, “Electrospun silk fibroin mats for tissue engineering,” *Eng. Life Sci.*, vol. 8, no. 3, pp. 219–225, 2008.

[20] S. Ghosh, S. T. Parker, X. Wang, D. L. Kaplan, and J. A. Lewis, “Direct-write assembly of microperiodic silk fibroin scaffolds for tissue engineering applications,” *Adv. Funct. Mater.*, vol. 18, no. 13, pp. 1883–1889, 2008.

[21] X. Zhang and Z. Pan, “Microstructure transitions and dry-wet spinnability of Silk fibroin protein from Waste silk quilt,” *Polymers (Basel).*, vol. 11, no. 10, 2019.

[22] G. G. Leisk, T. J. Lo, T. Yucel, Q. Lu, and D. L. Kaplan, “Electrogelation for protein adhesives,” *Adv. Mater.*, vol. 22, no. 6, pp. 711–715, 2010.

[23] S. D. Wang and K. Q. Zhang, “Electrogelation and rapid prototyping of Bombyx mori silk fibroin,” *Mater. Lett.*, vol. 169, pp. 5–9, 2016.

[24] X. Wang, J. A. Kluge, G. G. Leisk, and D. L. Kaplan, “Sonication-induced gelation of silk fibroin for cell encapsulation,” *Biomaterials*, vol. 29, no. 8, pp. 1054–1064, 2008.

[25] T. Yucel, P. Cebe, and D. L. Kaplan, “Vortex-induced injectable silk fibroin hydrogels,” *Biophys. J.*, vol. 97, no. 7, pp. 2044–2050, 2009.

[26] B. P. Partlow *et al.*, “Highly tunable elastomeric silk biomaterials,” *Adv. Funct. Mater.*, vol. 24, no. 29, pp. 4615–4624, 2014.

[27] A. Mazzocchi, M. Devarasetty, R. Huntwork, S. Soker, and A. Skardal, “Optimization of collagen type I-hyaluronan hybrid bioink for 3D bioprinted liver microenvironments,” *Biofabrication*, vol. 11, no. 1, 2019.

[28] K. S. Lim *et al.*, “Bio-resin for high resolution lithography-based biofabrication of complex cell-laden constructs,” *Biofabrication*, vol. 10, no. 3, 2018.

[29] K. S. Lim *et al.*, “One-Step Photoactivation of a Dual-Functionalized Bioink as Cell Carrier and Cartilage-Binding Glue for Chondral Regeneration,” *Adv. Healthc. Mater.*, vol. 9, no. 15, pp. 1–13, 2020.

[30] K. S. Lim *et al.*, “Visible Light Cross-Linking of Gelatin Hydrogels Offers an Enhanced Cell Microenvironment with Improved Light Penetration Depth,” *Macromol. Biosci.*,

vol. 19, no. 6, pp. 1–14, 2019.

[31] M. Grinstaff, “Photocrosslinkable polysaccharides forin situ hydrogel formation,” vol. 4636, no. January, 2018.

[32] M. Kesti *et al.*, “A versatile bioink for three-dimensional printing of cellular scaffolds based on thermally and photo-triggered tandem gelation,” *Acta Biomater.*, vol. 11, no. 1, pp. 162–172, 2015.

[33] S. H. Kim *et al.*, “Precisely printable and biocompatible silk fibroin bioink for digital light processing 3D printing,” *Nat. Commun.*, vol. 9, no. 1, pp. 1–14, 2018.

[34] L. Pescosolido *et al.*, “Hyaluronic acid and dextran-based semi-IPN hydrogels as biomaterials for bioprinting,” *Biomacromolecules*, vol. 12, no. 5, pp. 1831–1838, 2011.

[35] K. Dubbin, A. Tabet, and S. C. Heilshorn, “Quantitative criteria to benchmark new and existing bio-inks for cell compatibility,” *Biofabrication*, vol. 9, no. 4, 2017.

[36] E. A. Kamoun, A. M. Omer, M. M. Abu-Serie, S. N. Khattab, H. M. Ahmed, and A. A. Elbardan, “Photopolymerized PVA-g-GMA Hydrogels for Biomedical Applications: Factors Affecting Hydrogel Formation and Bioevaluation Tests,” *Arab. J. Sci. Eng.*, vol. 43, no. 7, pp. 3565–3575, 2018.

[37] H. H. Kim *et al.*, “Effect of silk fibroin molecular weight on physical property of silk hydrogel,” *Polymer (Guildf).*, vol. 90, pp. 26–33, 2016.

[38] X. Hu, D. Kaplan, and P. Cebe, “Determining Beta-Sheet Crystallinity in Fibrous Proteins by Thermal Analysis and Infrared Spectroscopy,” pp. 6161–6170, 2006.

[39] P. Bhattacharjee, J. Fernández-Pérez, and M. Ahearne, “Potential for combined delivery of riboflavin and all-trans retinoic acid, from silk fibroin for corneal bioengineering,” *Mater. Sci. Eng. C*, vol. 105, no. October 2018, p. 110093, 2019.

[40] S. Sharifi *et al.*, “Tuning gelatin-based hydrogel towards bioadhesive ocular tissue engineering applications,” *Bioact. Mater.*, vol. 6, no. 11, pp. 3947–3961, 2021.

[41] C. F. Guimarães, L. Gasperini, A. P. Marques, and R. L. Reis, “The stiffness of living tissues and its implications for tissue engineering,” *Nat. Rev. Mater.*, 2020.

[42] J. O. Buitrago *et al.*, “Silk fibroin/collagen protein hybrid cell-encapsulating hydrogels with tunable gelation and improved physical and biological properties,” *Acta Biomater.*, vol. 69, pp. 218–233, 2018.

[43] Y. P. Singh, A. Bandyopadhyay, and B. B. Mandal, “3D Bioprinting Using Cross-Linker-Free Silk-Gelatin Bioink for Cartilage Tissue Engineering,” *ACS Applied Materials and Interfaces*, vol. 11, no. 37. pp. 33684–33696, 2019.

[44] V. P. Ribeiro *et al.*, “Rapidly responsive silk fibroin hydrogels as an artificial matrix for

the programmed tumor cells death," *PLoS One*, vol. 13, no. 4, pp. 1–21, 2018.

[45] L. Z. Qiao-Na Wei, Ai-Min Huang, Lin Ma, Zilun Huang, Xi Huang, Pan-Pan Qiang, Zhu-Ping Gong, "Structure Regulation of Silk Fibroin Films for Controlled Drug Release," *J. Appl. Polym. Sci.*, 2012.

[46] X. Chen, Z. Shao, N. S. Marinkovic, L. M. Miller, P. Zhou, and M. R. Chance, "Conformation transition kinetics of regenerated Bombyx mori silk fibroin membrane monitored by time-resolved FTIR spectroscopy," *Biophys. Chem.*, vol. 89, no. 1, pp. 25–34, 2001.

[47] and C. C. P. David J. Belton, Robyn Plowright, David L. Kaplan, "A Robust Spectroscopic Method for the Determination of Protein Conformational Composition-Application to the Annealing of Silk," *Acta Biomater.*, vol. 73, pp. 355–364, 2018.

[48] I. Pepelanova, K. Kruppa, T. Scheper, and A. Lavrentieva, "Gelatin-methacryloyl (GelMA) hydrogels with defined degree of functionalization as a versatile toolkit for 3D cell culture and extrusion bioprinting," *Bioengineering*, vol. 5, no. 3, 2018.

[49] S. S. Silva *et al.*, "Silk hydrogels from non-mulberry and mulberry silkworm cocoons processed with ionic liquids," *Acta Biomater.*, vol. 9, no. 11, pp. 8972–8982, 2013.

[50] I. Pepelanova, K. Kruppa, T. Scheper, and A. Lavrentieva, "Gelatin-Methacryloyl (GelMA) Hydrogels with Defined Degree of Functionalization as a Versatile Toolkit for 3D Cell Culture and Extrusion Bioprinting," *Bioengineering*, vol. 5, no. 3. p. 55, 2018.

[51] H. Liang, S. J. Russell, D. J. Wood, and G. Tronci, "A hydroxamic acid-methacrylated collagen conjugate for the modulation of inflammation-related MMP upregulation," *J. Mater. Chem. B*, vol. 6, no. 22, pp. 3703–3715, 2018.

[52] G. Pitarresi, P. Pierro, F. S. Palumbo, G. Tripodo, and G. Giammona, "Photo-cross-linked hydrogels with polysaccharide-poly(amino acid) structure: New biomaterials for pharmaceutical applications," *Biomacromolecules*, vol. 7, no. 4, pp. 1302–1310, 2006.

[53] S. D. Aznar-Cervantes, A. A. Lozano-Perez, M. Garcia Montalbon, G. Villora, D. Vicente-Cervantes, and J. L. Cenis, "Importance of refrigeration time in the electrospinning of silk fibroin aqueous solutions," *J. Mater. Sci.*, vol. 50, no. 14, pp. 4879–4887, 2015.

[54] X. Cui *et al.*, "Rapid Photocrosslinking of Silk Hydrogels with High Cell Density and Enhanced Shape Fidelity," *Adv. Healthc. Mater.*, vol. 9, no. 4, 2020.

[55] and D. L. K. Kelly A. Burke†,‡,§, Dane C. Roberts‖, "Silk Fibroin Aqueous-Based Adhesives Inspired by Mussel Adhesive Proteins Kelly," *Biomacromolecules*, vol. 17, no. 1, pp. 237–245, 2016.

[56] D. Fischer, Y. Li, B. Ahlemeyer, J. Krieglstein, and T. Kissel, “Fischer-2003-In vitro cytotoxicit.pdf,” vol. 24, pp. 1121–1131, 2003.

[57] J. P. Mazzoccoli, D. L. Feke, H. Baskaran, and P. N. Pintauro, “Mechanical and Cell Viability Properties of Crosslinked Low and High MW PEGDA blends,” *J. Biomed. Mater. Res. A*, vol. 93, no. 2, pp. 558–566, 2010.

[58] L. Li *et al.*, “Gelatin-Based Photocurable Hydrogels for Corneal Wound Repair,” *ACS Appl. Mater. Interfaces*, vol. 10, no. 16, pp. 13283–13292, 2018.

[59] N. J. Chan *et al.*, “Spider-silk inspired polymeric networks by harnessing the mechanical potential of β-sheets through,” *Nat. Commun.*, no. 2020, pp. 1–14.

[60] A. Assmann *et al.*, “A highly adhesive and naturally derived sealant,” *Biomaterials*, vol. 140, pp. 115–127, 2017.

[61] H. Kim, M. N. Park, J. Kim, J. Jang, H. K. Kim, and D. W. Cho, “Characterization of cornea-specific bioink: high transparency, improved in vivo safety,” *J. Tissue Eng.*, vol. 10, 2019.

[62] B. Zhang *et al.*, “3D bioprinting for artificial cornea: Challenges and perspectives,” *Med. Eng. Phys.*, vol. 71, pp. 68–78, 2019.